Dyes and Pigments 244 (2026) 113112

Contents lists available at ScienceDirect

Dyes and Pigments

journal homepage: www.elsevier.com/locate/dyepig

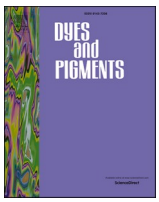

Smartphone-assisted RGB color analysis of a paper-based vapochromic chemosensor for selective detection of pyridine vapors

Massimiliano Gaeta *, Agostino Attinà, Ivan Pietro Oliveri, Santo Di Bella **

Dipartimento di Scienze Chimiche, Università di Catania, I-95125, Italy

ARTICLE INFO

Keywords:
Zn(II) Schiff-base complex
Vapochromic paper-based sensor
Pyridine vapor sensing
RGB color analysis

ABSTRACT

The search for simple and effective optical chemosensors is an area of current and growing interest. In this work, a paper-based chemosensor of a vapochromic Zn(salen)-type complex is developed. It can selectively detect pyridine vapors, from those of the most common VOCs and other heterocyclic amines, over a wide concentration range from tens to thousands of ppm, requiring a simple fabrication method, films preparation by dip-coating, and enabling detection by using a smartphone-assisted color recognition app and a proper RGB color analysis. The latter includes normalization to the rgb values and the color difference ΔE_{rgb}, from the RGB color changes of the films before and after exposure. Reliability of this method is assessed by comparison with results of UV–vis reflectance spectra, and could represent a general approach for VOCs detection using vapochromic materials on films. These results are contrasted with those obtained using non-normalized RGB values, demonstrating that the latter can lead to unreliable and hardly repeatable results. Vapochromic paper-based films represent a simple, cost-effective, portable and disposable chemosensor that, combined with a proper RGB color analysis readout, is useful for the on-site detection of pyridine vapors in various industrial and environmental settings.

1. Introduction

Stimuli-responsive chromic materials have attracted increasing attention due to their high potential in the development of chemical sensors and smart devices able of responding to external environmental stimuli by changing color [1–5]. Among them, paper-based chemosensors, obtained by supporting the chromic material on paper substrates, represent simple and efficient systems for sensing vapors of volatile compounds or gases, taking advantages of their facile fabrication and easy signal read-out [6–9]. In this regard, the detection of volatile organic compounds (VOCs), particularly those toxics and industrially relevant, such as nitrogen-containing VOCs (N–VOCs), such as pyridine (py) or aliphatic amines, is increasingly critical for both environmental monitoring and workplace safety [10]. Therefore, the development of new paper-based chemosensors is relevant to realize portable tools for on-site and real-time detection of harmful VOCs.

Pyridine is a volatile aromatic amine commonly found in industrial processes, including the synthesis of insecticides, pesticides, herbicides, pharmaceuticals, dyes, fragrances, rubber or adhesive additives [11–13]. Currently, the worldwide py production exceeds 20,000 tons per annum and, in these contexts, environmental analyses of emissions from some manufacturing industries have revealed high concentrations of py vapors ranging from hundreds to thousands of ppm [14,15]. However, py is toxic by inhalation, ingestion, or skin absorption, leading to acute symptoms of intoxication [16–19]. Therefore, its release into the environment during synthetic processes can represent a significant risk to environmental safety and human health [20,21]. In light of this, the development of methods that enable for simple and sensitive detection of py levels over a wide concentration range is not only desirable but essential to mitigate exposure risks [22].

In recent years, the detection of py vapors has been explored through various strategies, by using small molecules [23–25], perovskite functional dyes [26], metal-organic frameworks [27,28], supramolecular organic frameworks [29], fullerenes [30], nanoparticles [31], polymeric materials, such as hybrid polymers [32,33] and polyazobenzenes [34], or sensor-array based on cationic conjugated polymers with various counter-anions [35]. Other studies have involved vapochromic and vapoluminescent materials [36–43].

Among these strategies for detection of py vapors, vapochromic materials represent highly desirable chemosensors for the rapid, on-site

* Corresponding author.
** Corresponding author.
E-mail addresses: massimiliano.gaeta@unict.it (M. Gaeta), sdibella@unict.it (S. Di Bella).

https://doi.org/10.1016/j.dyepig.2025.113112
Received 4 June 2025; Received in revised form 24 July 2025; Accepted 8 August 2025
Available online 8 August 2025

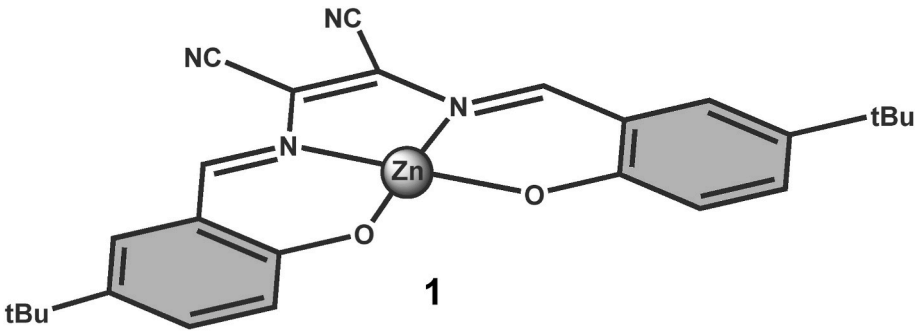

Fig. 1. Molecular structure of complex **1**.

detection, thanks to their ability to undergo color changes, visible even to the naked eye, without the need for complex instrumentation. However, most of vapochromic systems reported for detection of py vapors have been involved in qualitative detection, or without demonstrating their selectivity [37–40,43].

Lewis acidic Zn(II) salen-type complexes [44–47] have recently been studied for their ability to form adducts with volatile Lewis bases, resulting in remarkable vapochromic and vapoluminescence responses [48–51], and responsive nanostructures [44,45,52–57]. In particular, the Zn(salmal) complex **1** (Fig. 1) exhibits a unique thermochromic and vapochromic behavior, also enabling the detection of various VOCs after exposure to their saturated vapors [48].

Within this context, in the present paper we developed vapochromic paper-based films of complex **1** capable of selectively detecting py vapors from those of most common VOCs over a wide concentration range, requiring a simple fabrication method and enabling their detection by using a smartphone-assisted color recognition app and a proper and accurate RGB color analysis, thus representing feasible chemosensors useful for on-site detection of py vapors in various industrial and environmental contexts.

2. Experimental section

2.1. Materials and physical measurements

All of the chemicals used were purchased from Sigma-Aldrich (Merk Life Science S.r.l., Milano, Italy) and used as received, with the exception of pyrrole and pyrrolidine, which were purified by fractional distillation at atmospheric pressure over calcium hydride. Complex **1** was synthesized and characterized according to the procedure previously reported [58] and dried under vacuum at 100 °C before use. UV–vis diffuse reflectance spectra on paper-based films were recorded with a JASCO V-750 spectrophotometer.

2.2. Preparation of paper-based films, storage, and vapor exposure experiments

Paper-based films were prepared via dip-coating technique, by dipping Whatman-4 paper, cut in 2.5 cm × 2.5 cm squares, for few seconds in THF solutions of **1** under a nitrogen atmosphere in a flask. 1.0 mM and 0.4 mM THF solutions were used to prepare films named G-1 and G-04, respectively. After the dipping process, the films were kept horizontal and dried by evaporation of the solvent at room temperature under a nitrogen atmosphere. Finally, the films were stored in a flask in the dark at room temperature kept under inert atmosphere before their use. Paper-based films stored at room temperature (22 ± 3 °C) with a relative humidity (RH) in the range of 40–60 % and low lighting levels (<500 lux), remain quite stable over time, as monitored by the reflectance spectra (measurements up to five weeks). Conversely, higher RH (>70 %) and/or higher illumination levels (>2000 lux), lead to a significant reduction in the absorbance intensity of the films, especially in the region of interest (400–700 nm), only after a few days.

Exposure experiments of paper-based films, freshly-prepared or stored under inert atmosphere, to known ppm vapor concentrations of the investigated VOCs were performed under static conditions. The experimental setup for the static exposure experiments and the details of the static liquid–gas distribution method to calculate the desired ppm concentration of the VOCs involved have been previously described [49]. Exposure to vapor concentrations below 500 ppm was performed by injection into the sealed chamber (1.15 L), solutions of the involved VOCs in pentane (b.p. 36.1 °C) with a concentration of 0.0473 M, allowing their complete evaporation. This concentration was chosen such that 1 μL of the 0.0473 M solution injected into the sealed chamber is equal to a concentration of 1 ppm. For vapor concentrations ≥500 ppm, appropriate volumes of pure VOCs were injected into the sealed chamber, allowing their complete evaporation. The exposure time was set at 90 min for each VOC investigated, at room temperature (22 ± 3 °C) with a RH in the range of 40–60 %. This exposure time ensures that both the maximum color change and saturation of the absorbance intensity for each exposed film are achieved over the entire concentration range investigated. Exposure experiments using paper-based films stored under indoor conditions (temperature = 22 ± 3 °C; RH = 50 ± 10 %, illuminance <500 lux) gave analogous optical responses (measurements up to five weeks).

2.3. RGB color analysis

RGB color analysis of paper-based films was performed on digital images. Photographic images of the films were taken under defined illumination conditions (see text) by using a smartphone camera placed at a constant distance from the film (15 cm). Then, the photographs were exported as jpeg files. RGB values of each sample film were acquired by an android app (*Color Detector* developed by Galaxy studio apps). Note that RGB colors captured directly on the films or from their digital images gave similar RGB values. Normalized rgb values were calculated according to equations (2–4) (section 3.2.). Mean RGB or rgb values were calculated from at least three replicate measurements. ΔE_{RGB} and ΔE_{rgb}, were calculated according to equation (5) (section 3.2.) from the raw RGB and their normalized rgb colors, respectively.

2.4. Calculation of the limit of detection

The LOD of G-04 films for py vapors, from UV–vis reflectance spectral data, was calculated in the dynamic linear range with the following formula:

$$LOD = K \times \frac{S_b}{S} \quad (1)$$

where K is a constant, S_b is the standard deviation of the blank, calculated from the absorbance intensity at 560 nm of over 20 films, and S is the slope derived from the linear fit curve. The calibration curve was obtained from the plot of the absorbance intensity at 560 nm versus the

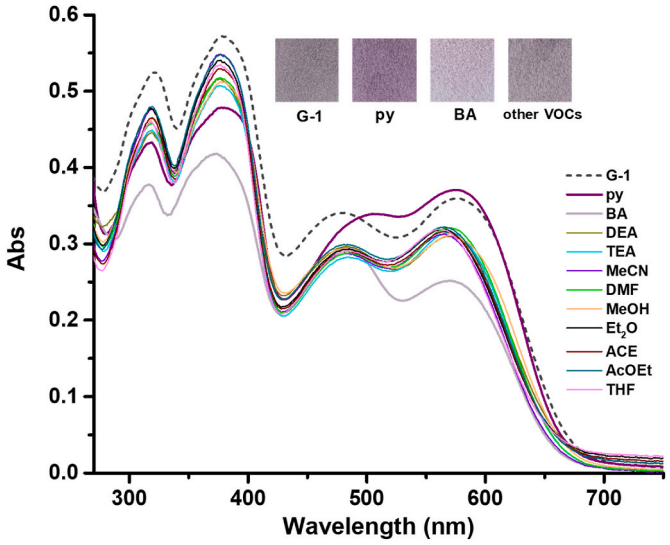

Fig. 2. UV–vis reflectance spectra of a G-1 film, from 1.0 mM THF solutions of **1**, before and after static exposure to a vapor concentration of 1000 ppm of various VOCs. Inset: photographic images of G-1 films before and after exposure to a vapor concentration of 1000 ppm of the VOCs involved.

increasing concentration of py. Each point of the calibration curve is related to the mean value obtained from at least three replicate measurements. Using eq. (1), with $K = 3$, $S_b = 1.13 \times 10^{-3}$ and $S = 3.61 \times 10^{-5}$, a LOD value of 94 ppm was calculated. Analogously, the LOD of G-04 films for py vapors, from mean ΔE_{rgb} data and linear fit ($S = 5.61 \times 10^{-5}$), each mean value from at least three replicate measurements, was calculated using a standard deviation of the blank of 6.75×10^{-4}, from $n \geq 30$ replicates (LOD = 36 ppm). The LOD of G-1 films for py vapors, from mean ΔE_{rgb} data and related linear fit ($S = 1.67 \times 10^{-5}$), each mean value from at least three replicate measurements, was calculated using a standard deviation of the blank of 3.22×10^{-3}, from $n \geq 30$ replicates (LOD = 578 ppm).

3. Results and discussion

3.1. Chromic response of paper-based films

We have previously demonstrated that the Zn(salmal) complex **1** possesses remarkable thermochromic and vapochromic properties [48]. The red-brown solid of **1**, obtained by complete solvent evaporation in air from their THF solutions, shows a marked thermochromism associated with a phase transition. Instead, the dark-gray solid of **1**, obtained by evaporation of the solvent under anhydrous conditions, has a different lattice structure and does not exhibit thermochromism or phase transition. Furthermore, the anhydrous complex **1**, as solid or in cast films, shows a distinctive optical response upon exposure to saturated vapors of some volatile N–VOCs and oxygenated VOCs (OVOCs). In particular, while exposure to saturated vapors of primary amines, such as isopropylamine or butylamine (BA), leads to an irreversible color change, from gray to yellow, with demetalation of **1** [48], after exposure to saturated vapors of py the anhydrous powders or films of **1** show a vapochromic behavior with a significant color change, from gray to purple, associated with the formation of stoichiometric 1:1 adducts, **1**·py [48]. Finally, the anhydrous films of **1** when exposed to secondary and tertiary aliphatic amines or OVOCs, become red-brown [48].

The interesting chromic properties of this molecular material prompted us to further investigate its sensing and selective response to certain concentrations of VOCs vapors. To this end, the anhydrous complex **1** was deposited by the dip-coating technique onto paper substrates from 1.0 mM THF solutions of **1**, see experimental section for details, obtaining gray (G-1) films (Fig. 2). This procedure ensures optical homogeneity and repeatability of the films, a prerequisite for quantitative detection studies. Films remain stable for several months if stored in the dark, at room temperature and under inert atmosphere. Temporal stability studies of G-1 films, by monitoring the absorption bands in the UV–vis reflectance spectra, indicate that they can be stored even under indoor conditions, i.e., room temperature (22 ± 3 °C), RH (50 ± 10 %), and low lighting levels (500 lux), without appreciable optical changes. This suggests that the films exhibit sufficient stability under standard storage conditions allowing for their use in real-world applications.

The optical response of G-1 films was evaluated after static exposure to defined vapor concentrations of various VOCs. In particular, a series

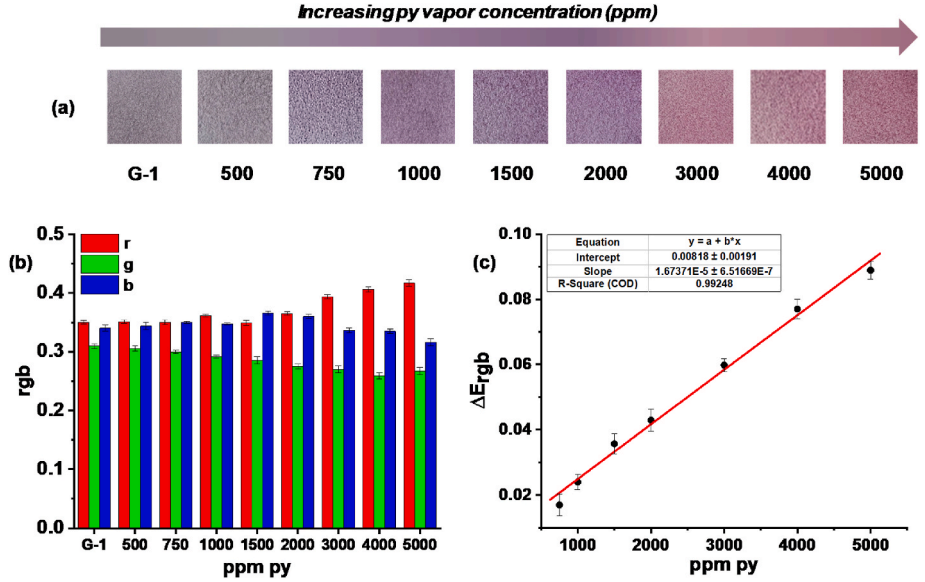

Fig. 3. (a) Photographic images of G-1 films before and after exposure to increasing concentrations of py. (b) Mean rgb values of G-1 films before and after exposure to py vapors. (c) Mean ΔE_{rgb} values as a function of py vapor concentration and the related linear best fit (red line). Error bars indicate standard deviation of the means.

of volatile compounds representative of principal classes (reported in parentheses) of N–VOCs and OVOCs were considered: BA (primary aliphatic amines), diethylamine (DEA, secondary aliphatic amines), triethylamine (TEA, tertiary aliphatic amines), py (heterocyclic aromatic amines), acetonitrile (MeCN, nitriles), *N*,*N*-dimethylformamide (DMF, amides), methanol (MeOH, alcohols), diethyl ether (Et_2O, ethers), tetrahydrofuran (THF, cyclic ethers), acetone (ACE, ketones), and ethyl acetate (AcOEt, esters).

Initially, a vapor concentration of 1000 ppm was chosen. The optical response of G-1 films, after static exposure to a vapor concentration of 1000 ppm for each of VOCs involved is quite different. The reflectance spectrum of G-1 films in the visible region is characterized by two absorption bands, centered at 480 nm and 575 nm, responsible for its gray color (Fig. 2). After static exposure to 1000 ppm of py, G-1 films turn grape in color, with the formation of a new band at ca. 505 nm and a slight increase of the absorption band at 575 nm (Fig. 2). In contrast, exposure of G-1 films to 1000 ppm of BA, leads to an overall decrease in the intensity of absorption bands in the reflectance spectrum, compared to that of pristine G-1 films, particularly pronounced that at 575 nm, consistent with the observed color change (discolor) of the exposed film (Fig. 2). On the other hand, exposure of G-1 films to a vapor concentration of 1000 ppm of all other involved VOCs does not give significant color changes, as also indicated by reflectance spectra similar to those of pristine G-1 films (Fig. 2).

To further investigate the optical response of G-1 films towards other volatile heterocyclic amines, alicyclic amines (piperidine, pyrrolidine), heterocyclic aromatic amines (pyrrole) and pyridine derivatives (2-methylpyridine or α-picoline, 4-methylpyridine or γ-picoline, 2,6-dimethylpyridine or α,α′-lutidine) were considered. Exposure of G-1 films to a vapor concentration of 1000 ppm for each of these heterocyclic amines results in a different optical response (Fig. S1). In particular, alicyclic amines and pyrrole behave like the above involved VOCs, as no significant changes in the color of the films are observed after exposure. Pyridine derivatives, on the other hand, are characterized by a different optical response, with 4-methylpyridine behaving like py, while 2-methylpyridine and 2,6-dimethylpyridine, even involving some reflectance spectral changes, do not give rise to significant color changes.

It therefore turns out that G-1 films of the anhydrous complex **1** can selectively detect py vapors, from the most common VOCs and other volatile heterocyclic amines, except 4-methylpyridine, at a vapor concentration of 1000 ppm, which represents the immediately dangerous to life or health (IDLH) air concentration for py, established by the National Institute for Occupational Safety and Health [59]. Moreover, under these conditions, G-1 films also appear to be partly responsive to BA.

On the basis of the optical response of G-1 films to the vapor concentration of 1000 ppm, studies were then performed by varying the py and BA vapor concentration. Fig. 3a shows the photographs images of G-1 films after exposure to various vapor concentrations (500–5000 ppm) of py, the related reflectance spectra are reported in the SI (Fig. S2). While exposure to a py vapor concentration of 500 ppm does not lead to significant color changes in the G-1 films, for vapor concentrations $\geq$750 ppm a defined, gradual visual color change, from gray to purple is observed. Instead, exposure of G-1 films to BA vapors results in a significant color change to yellow-brown at vapor concentrations $\geq$2000 ppm, becoming yellow at a vapor concentration of 3000 ppm, due to an almost complete demetalation of the complex (Fig. S3). Therefore, these naked-eye color changes of G-1 films are useful for detecting the presence of py vapors within these concentration ranges (500–5000 ppm), and for discriminatively detecting BA vapors at concentrations $\geq$2000 ppm.

3.2. Detection of py vapors by smartphone-assisted RGB color analysis

The rich visual color changes observed after exposure of G-1 films to increasing concentrations of py vapors provide a broad space for the design and development of simple detection tools to quantitatively determine on-site the presence of this analyte [60]. In particular, by using portable electronic devices, such as a smartphone, the chromic response of the paper-based films can be represented in the RGB color space [61], composed by three channels, red (R), green (G), and blue (B), with pixel intensity values ranging from zero to 255 (8-bit for each color channel). Therefore, smartphone-assisted RGB color analysis of G-1 films before and after exposure to py vapors was performed, whose RGB color was captured using a color recognition android app (*Color Detector* developed by Galaxy studio apps).

However, RGB values are device-dependent and very sensitive to illumination changes, such as shadows or shines, making color analysis difficult [61,62]. To overcome these problems, the standard RGB color space can be converted into normalized RGB color space, denoted rgb [62,63]. Thus, the raw RGB values acquired from G-1 films were then transformed into normalized rgb, through equations (2-4), and used for further analysis.

$$r = \frac{R}{R+G+B} \tag{2}$$

$$g = \frac{G}{R+G+B} \tag{3}$$

$$b = \frac{B}{R+G+B} \tag{4}$$

Color analysis of G-1 films (Fig. 3a), before and after exposure to different concentrations of py vapors (500–5000 ppm), was performed capturing RGB values by the *Color Detector* app at an almost constant lighting (1600–2000 lux) using a Samsung Galaxy S23 smartphone. Given the very good optical homogeneity of G-1 films, it was not necessary to average the RGB values captured from the different areas, as the same values were obtained. On the other hand, RGB color captured directly on the films or from their digital images yielded the same results. At least three replicates were performed using this procedure, obtaining mean RGB values which were then normalized to rgb values (Fig. 3b).

As G-1 films after exposure involve a color change, their color analysis can conveniently be expressed as the color difference before and after exposure, as the Euclidean distance (ΔE) between two points in space representing the two RGB colors (eq. (5)), and can be used for both raw RGB and normalized rgb colors [61,64]:

$$\Delta E_{RGB} = \sqrt{\Delta R^2 + \Delta G^2 + \Delta B^2} \tag{5}$$

where ΔR, ΔG, ΔB, represent the difference between the R, G, B, or their normalized values, before and after exposure to a given vapor concentration.

Indeed, for G-1 films, among the various relationships between the rgb values and py vapor concentration, the color difference before and after exposure best describes the observed color changes, while all the other relationships are weaker or not significant (Figs. S4 and S5). Thus, the color difference, ΔE_{rgb}, as a function of py vapor concentration indicates a strong linear relationship ($R^2 = 0.992$) over a vapor concentration range up to 5000 ppm (Fig. 3c). These data also enable the calculation of the limit of detection (LOD) for py vapors using G-1 films and their rgb color analysis. Hence, from data of Fig. 3c and the standard deviation of the blank (n $\geq$ 30 replicates) an estimated LOD of 578 ppm is obtained.

The normalized RGB color space is effective in color analysis of G-1 films under different lighting conditions and even using different smartphones, resulting in comparable normalized rgb values. This was demonstrated by performing an independent set of experiments in which the RBG values were captured from digital images of G-1 films before and after exposure to different concentrations of py vapors (1000 ppm, 3000 ppm, 5000 ppm) under two lighting conditions, 1800 lux and 30 lux, and using three different smartphones, Samsung Galaxy S23,

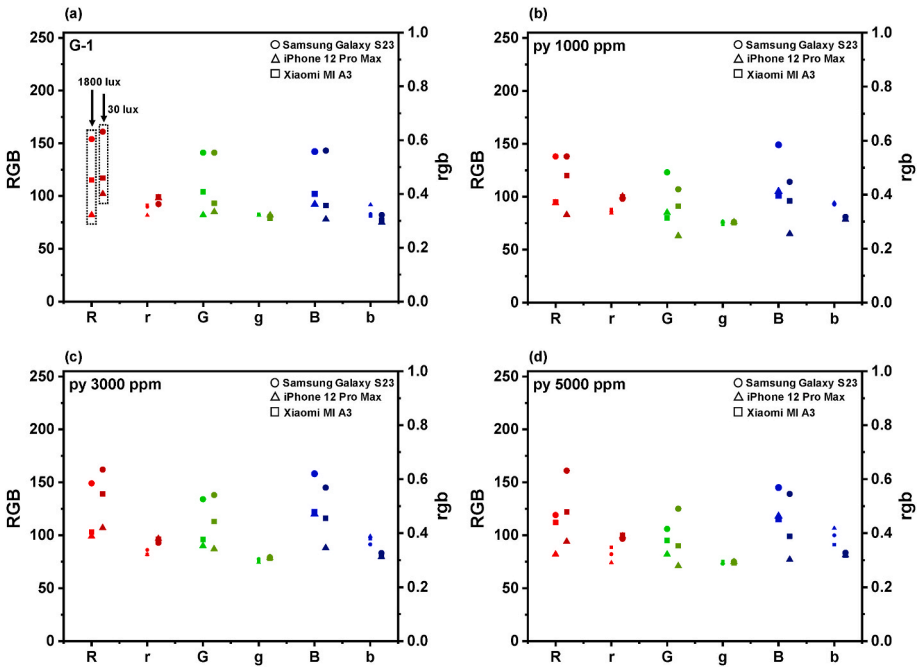

Fig. 4. RGB values of G-1 films before (a) and after exposure to different concentrations of py vapors (b–d) captured with three different smartphones and under two different lighting conditions, 1800 lux and 30 lux (as indicated in (a)), and their normalized rgb values.

Xiaomi MI A3, and iPhone 12 Pro Max. It was found that captured RGB values are very different from each other, both between the two lighting conditions and between the different smartphones (Fig. 4). Nevertheless, RGB normalization returns comparable rgb values, both in the two lighting conditions and between the different smartphones (Fig. 4). Furthermore, using mean rgb values from this set of data, the color difference, ΔE_{rgb}, as a function of py vapor concentration indicates a linear relationship (Fig. S6), with the slope of the linear best fit nearly identical to that obtained above (Fig. 3c) from the different set of replicate measurements using a same smartphone (Samsung Galaxy S23) under nearly constant illumination conditions (1600–2000 lux).

These results are truly impressive because they demonstrate that using a simple approach and a proper analysis, i.e. smartphone-assisted RGB color analysis of the G-1 films before and after exposure, then normalization to the rgb values, and finally the color difference ΔE_{rgb}, allows for accurate detection of py vapors in the concentration range of 750–5000 ppm.

In this context, it is also instructive to consider the non-normalized RGB values to check whether their RGB analysis is suitable to adequately quantify the py vapor concentration. Using mean RGB values of the same set of data used for the rgb analysis in Fig. 3, the color difference, ΔE_{RGB}, as a function of py vapor concentration also gives a strong linear relationship ($R^2 = 0.997$) over a vapor concentration range of 750–5000 ppm (Fig. S7), but with an increased standard deviation of the mean values. Therefore, RGB color analysis, whose RGB values are captured by a smartphone under nearly constant lighting, followed by the color difference, ΔE_{RGB}, apparently leads to similar results. However, in this case the derived LOD is 425 ppm, which certainly represents an unreliable value, since at this concentration of py vapors the G-1 films are not responsive (Fig. 3 and S2).

Therefore, care must be taken when analyzing RGB data for sensing applications, otherwise unreliable results may be obtained. In any case, smartphone-assisted RGB color analysis using non-normalized RGB values, even if performed under standardized conditions, especially in term of illumination which, unfortunately, is almost never indicated, would be device-dependent, and therefore its repeatability remains rather limited.

In summary, no difficult measurement or complex instrumentation

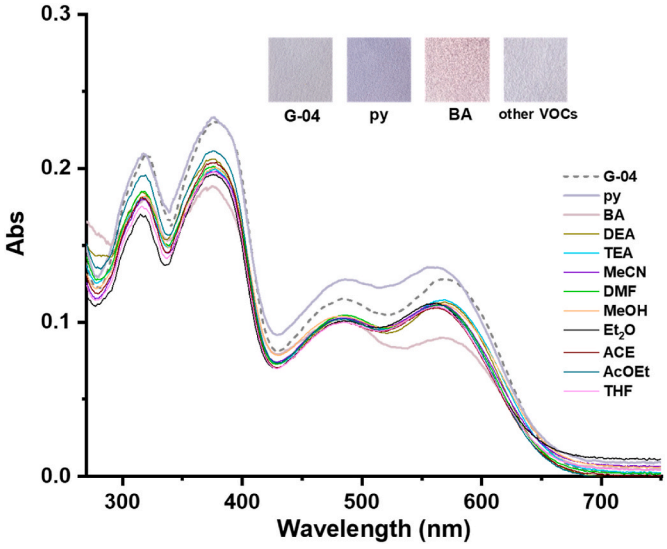

Fig. 5. UV–vis reflectance spectra of a G-04 film, from 0.40 mM THF solutions of **1**, before and after static exposure to a vapor concentration of 300 ppm of various VOCs. Inset: photographic images of G-04 films before and after exposure to a vapor concentration of 300 ppm of the VOCs involved.

are necessary to reveal the presence of py at these concentrations, as it can be identified by the naked eye with the color change of films, and quantitatively detected by a smartphone-assisted color recognition app and a proper RGB color analysis. Hence, G-1 films are suitable chemosensors useful for detection of py vapors. In particular, G-1 films selectively detect py vapors from those of most common VOCs at the IDLH concentration (1000 ppm) and up to concentrations of 5000 ppm. On the other hand, G-1 films, at higher concentrations ≥2000 ppm, in addition to py vapors, also discriminately detect primary amine vapors. These vapor concentrations are useful in industrial and environmental settings for workplace safety and environmental monitoring [18,65].

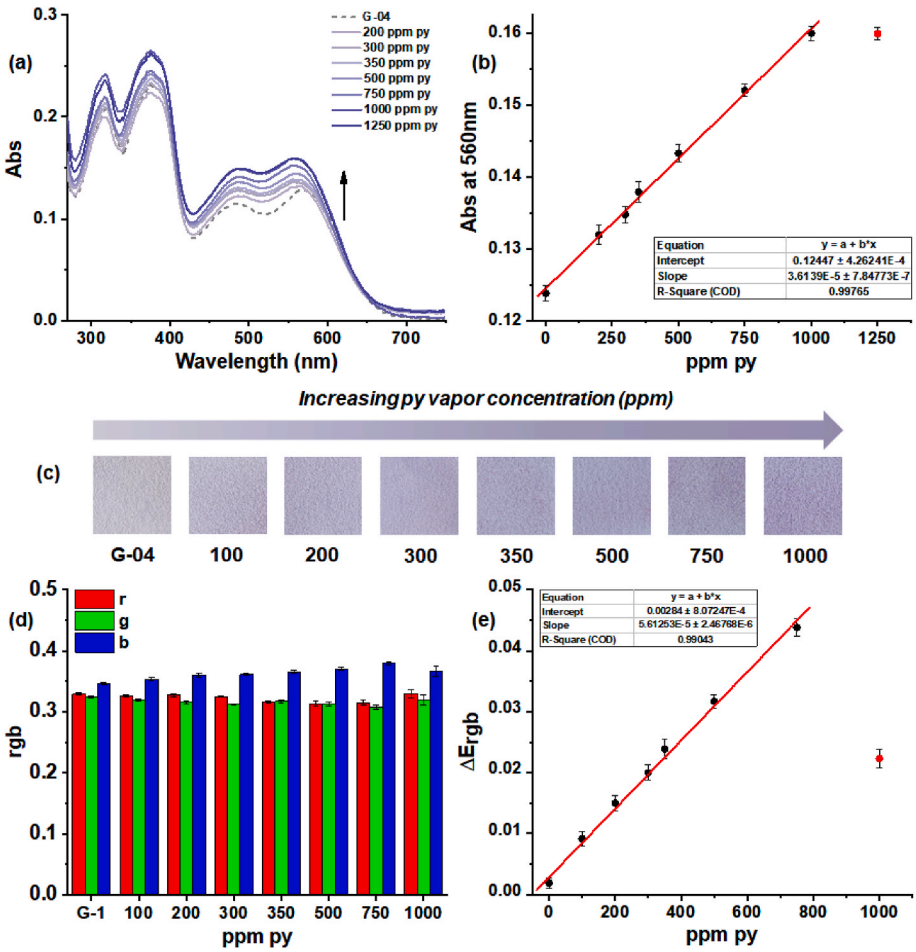

Fig. 6. (a) UV–vis reflectance spectra of G-04 films before and after exposure to an increasing concentration of py vapors. Each spectrum was recorded in an independent experiment. (b) Variation of the absorbance at 560 nm as a function of the concentration of py vapors and linear best fit in the linear dynamic range. (c) Photographic images of G-04 films before and after exposure to increasing concentrations of py vapors. (d) Mean rgb values of G-04 films before and after exposure to py vapors. (e) Mean ΔE_{rgb} values as a function of concentration of py vapors and the related linear best fit (red line). The data points at 1250 ppm in (b) and 1000 ppm in (e), marked in red, are not included in the linear fit. Error bars indicate standard deviation of the means.

3.3. Sensitive detection of py vapors

Based on these results, we decided to evaluate the optical response of further paper-based films, prepared using the same procedure but from THF solutions of **1** with lower concentrations, trying to improve their sensitivity. In particular, a concentration of 0.40 mM was chosen, obtaining paler gray (G-04) films. Reflectance spectra G-04 films (Fig. 5) in the visible region are characterized by two absorption bands, slightly shifted compared to those found in G-1 films (Fig. 2), with maxima at 484 nm and 568 nm. After static exposure to a vapor concentration of 300 ppm of py and the other VOCs involved above, significant changes in absorbance, similar to those found for G-1 films, are observed only for py and BA. In particular, in the case of exposure to py vapors, an increase in the intensity of the absorption bands at 484 nm and at 568 nm is observed, the latter blue-shifted at 560 nm. While, after exposure to BA vapors, an overall decrease in the absorbance intensity of the reflectance spectrum is observed, compared to that of G-1 films, more pronounced the in band at 568 nm. Consequently, a noticeable color change of G-04 films is observed after exposure to py and BA vapors, from pale-gray to violet and lilac, respectively. Again, considering the volatile heterocyclic amines involved above, exposure of G-04 films to a vapor concentration of 300 ppm of these amines shows similar behavior to that observed after exposure to 1000 ppm (Fig. S8). Therefore, G-04 films behave as G-1 films, in terms of selective detection of py and BA vapors from all other VOCs involved, but with significantly improved sensitivity as they are responsive to lower vapor concentrations (300 ppm).

Static exposure experiments were then performed using G-04 films exposed to various py vapor concentrations and the changes in UV–vis reflectance spectra were evaluated. Exposure to increasing concentrations of py vapors, leads to a progressive increase of the optical absorption bands at 484 nm and 560 nm (Fig. 6a), resulting in a progressively more marked color change to violet of the G-04 films (Fig. 6c). Saturation occurs after exposure to a concentration of ca. 1000 ppm of py vapors. The absorbance at 560 nm as a function of py vapors concentration shows a linear dynamic range up to 1000 ppm, with a very good linearity coefficient ($R^2 = 0.998$) (Fig. 6b). This allows establishing a LOD of 94 ppm.

On the other hand, exposure of G-04 films to BA vapors, within the same concentration range (100–1000 ppm), reveals that they are responsive to concentrations ≥300 ppm (lilac colored), becoming completely demetalated (yellow films) at 1000 ppm (Fig. S9). Therefore, G-04 films are useful for detecting the presence of py vapors up to 750 ppm, and for discriminatively detecting BA vapors at concentrations ≥300 ppm.

Again, color analysis of G-04 films, before and after exposure to different concentrations of py vapors (100–1000 ppm), was performed by the *Color Detector* app at an almost constant lighting (1600–2000 lux) using a Samsung Galaxy S23 smartphone. Captured RGB colors were then normalized to rgb values (Fig. 6d). The color difference, ΔE_{rgb}, as a

Table 1
Comparison of the sensing performance of G-1 and G-04 films with that of other materials previously reported for the detection of pyridine vapors.

Material	Detection method	Linear range (ppm)	LOD (ppm)	Selectivity	Portability	Reference
Metal-phthalocyanines/sol-gel glasses	Chemiresistive	1–3	0.0079	no	moderate	[23]
Azacyclobutane modified Perylene Bisimide derivatives/glass	Chemiresistive	0.375–7500	0.375	no	moderate	[24]
Graphene/PEVA	Chemiresistive	28–138 ppm	not available	yes	moderate	[33]
MIL-101(Cr)-MOF	Piezoelectric	5–50	1.603	yes	low	[27]
Nanoscale MOF	Piezoelectric	0.3–25	0.04	yes	low	[28]
Cucurbit[10]uril-SOF	Fluorometric	not available	4–5	yes	moderate	[29]
Polycarbonate with side-chain dipolar chromophores	MZI waveguide	0–400	0.476	yes	moderate	[32]
Conjugated semiconducting polymers	Fluorometric	not available	33	yes	moderate	[35]
Copper(I)-cluster/paper	Fluorometric	2000–12000	344	yes	moderate	[36]
Zinc(II)porphyrin-containing polyimide nanofibrous membrane	Colorimetric and Fluorometric	0–50	0.041	yes	moderate	[41]
Heteroleptic copper(I) complex/paper	Fluorometric	1000–10000	722	yes	moderate	[42]
Cobalt(II) complex/PVC	Optical fiber	18–66	1	not available	moderate	[43]
Zinc(II) Schiff base complex/paper (**G-1**)	RGB color analysis	750–5000	578	yes	high	*this work*
Zinc(II) Schiff base complex/paper (**G-04**)	RGB color analysis	0–750	36	yes	high	*this work*

function of py vapor concentration indicates a very good linear relationship (R^2 = 0.990), hence a linear dynamic range, over a vapor concentration range up to 750 ppm (Fig. 6e). Moreover, an estimated LOD of 36 ppm is obtained.

Interestingly, the results obtained for G-04 films exposed to py vapors using both approaches, UV–vis reflectance spectra and RGB color analysis with the procedure described above, are consistent with each other, thus validating this RGB method. Indeed, since RGB color analysis involves the overall spectral changes of G-04 paper-based vapochromic films, it turns out to be more sensitive in detecting py vapors than that performed on the basis of optical absorption changes at a specific λ_{max}. Therefore, this further demonstrates the efficiency of the present RGB color analysis approach for detection studies involving vapochromic materials.

Another interesting aspect is related to the improved sensitivity to py vapors of the paper-based G-04 films deposited by the dip-coating technique from a more dilute THF solution of complex **1**, thus demonstrating that it is possible to modulate the sensitivity of the chemosensor, and hence its linear dynamic range, by varying the amount of material deposited on the substrate.

Overall, the combination of G-04 (dynamic linear range up to 750 ppm) and G-1 (dynamic linear range 750–5000 ppm) films enables the selective detection of py vapors over a very broad vapor concentration range, from tens to thousands of ppm. Additionally, our paper-based chemosensor combined with smartphone-assisted RGB color analysis ensure high portability for on-site detection. These features constitute a unique example among the chemosensors reported in the literature for the detection of pyridine vapors [23–43]. In fact, most of reported optical [25,26,34] and vapochromic/vapoluminescent [37–40] chemosensors do not include quantitative data. On the other hand, chemosensors for the quantitative detection of py vapors (Table 1), based on optical [29,32,35,36,41–43], chemiresistive [23,24,33] or piezoelectric [27,28] response, mostly have a limited dynamic linear range [23,27,28,41,43] or are not selective [23,24,43], furthermore they require expensive and benchtop instrumentation, which affects the portability in real-world applications for on-site monitoring.

As previously demonstrated, the sensing mechanism for the detection of py vapors using films of the anhydrous complex **1** can be related to the formation of stable 1·py adducts [48]. The selectivity of G-04 and G-1 films for py vapors with respect to the principal classes of N–VOCs, with the exception of primary amines for vapor concentrations above 300 ppm and 2000 ppm, respectively, where a demetalation occurs [48], may be related to the strong Lewis basicity and less steric hindrance on the donor atom of py compared to that of sterically encumbered secondary and tertiary amines, including alicyclic amines [66]. The steric hindrance caused by the α methyl(s) substituent(s) is also responsible for the behavior observed for the pyridine derivatives involved in this study. On the other hand, OVOCs are characterized by a lower Lewis basicity than N–VOCs [66], thus having a lower propensity to form stable adducts.

4. Conclusions

This investigation reports a simple and effective approach using paper-based films of a vapochromic Zn(salen)-type complex for the selective detection of py vapors, from those of the most common VOCs and other heterocyclic amines, over a very broad vapor concentration range, from tens to thousands of ppm. The dip-coating technique allows the fabrication of optically homogeneous paper-based films and, by acting on the concentration of the Zn(salen) complex in solution, it is possible to modulate their sensitivity, and therefore the linear dynamic range, by varying the amount of material deposited on the substrate.

The vapochromic response of paper-based films to py vapors results in appreciable visual color changes. Smartphone-assisted RGB color analysis of the films before and after exposure, then normalization to the rgb values and finally the color difference ΔE_{rgb}, allows for accurate, quantitative detection of py vapors. The results of the RGB analysis are assessed in comparison with those obtained from the UV–vis reflectance spectra, being consistent with each other. Therefore, without the need for any complex instrumentation or sophisticated measurements, a proper smartphone-assisted RGB color analysis could represent a general approach for the detection of VOCs using vapochromic materials on films. On the other hand, this study demonstrates that smartphone-assisted RGB color analysis for sensing applications using non-normalized RGB values can lead to unreliable and hardly repeatable results.

Overall, these paper-based vapochromic films represent a simple, cost-effective, reliable, portable, and disposable chemosensor that, combined with a proper RGB color analysis readout, is useful for on-site detection of pyridine vapors in various industrial and environmental settings.

CRediT authorship contribution statement

Massimiliano Gaeta: Writing – review & editing, Writing – original draft, Methodology, Investigation, Formal analysis, Conceptualization. **Agostino Attinà:** Validation, Methodology, Investigation, Formal analysis. **Ivan Pietro Oliveri:** Validation, Methodology, Investigation, Formal analysis. **Santo Di Bella:** Writing – review & editing, Writing – original draft, Validation, Supervision, Methodology, Formal analysis, Conceptualization.

Declaration of competing Interest

The authors declare that they have no known competing financial interests or personal relationships that could have appeared to influence the work reported in this paper.

Acknowledgements

This work was supported by the University of Catania, PIACERI 2024/2026, Linea di Intervento 1, and partially funded by European Union (NextGeneration EU), through the MUR-PNRR project SAMOTHRACE (ECS00000022). We gratefully thank Dr. A. Auditore (University of Catania) for his support in the UV–vis reflectance measurements.

Appendix. A Supplementary data

Supplementary data to this article can be found online at https://doi.org/10.1016/j.dyepig.2025.113112.

Data availability

Data will be made available on request.

References

[1] Razzaghi D, Babazadeh-Mamaqani M, Babaie A, Esmati F, Roghani-Mamaqani H, Rezaei M, De Clerck K, Hoogenboom R. Chromic Electrospun polymer nanofibers: preparation, applications, and the future. ACS Appl Mater Interfaces 2025;17:4247–89. https://doi.org/10.1021/acsami.4c17105.
[2] Li L, Li S-H, Li Z-Y, Zhang N-N, Yu Y-T, Zeng J-G, Hua Y. Advances in viologen-based stimulus-responsive crystalline hybrid material. Coord Chem Rev 2024;518:216064. https://doi.org/10.1016/j.ccr.2024.216064.
[3] Huang G, Du X, Boa H, Shi Li B. Colorful variation of tetraphenylethene derivatives in the solid state. Mater Chem Front 2024;8:104–32. https://doi.org/10.1039/D3QM00621B.
[4] Zeng S, Sun H, Park C, Zhang M, Zhu M, Yan M, Chov N, Li E, Smith AT, Xu G, Li S, Hou Z, Li Y, Wang B, Zhang D, Sun L. Multi-stimuli responsive chromism with tailorable mechanochromic sensitivity for versatile interactive sensing under ambient conditions. Mater Horiz 2020;7:164–72. https://doi.org/10.1039/C9MH00851A.
[5] Wenger OS. Vapochromism in organometallic and coordination complexes: chemical sensors for volatile organic compounds. Chem Rev 2013;113:3686–733. https://doi.org/10.1021/cr300396p.
[6] Feng L. Paper-based optical chemosensors. Elsevier; 2024. https://www.sciencedirect.com/book/9780443133565/paper-based-optical-chemosensors.
[7] Malik S, Singh J, Saini K, Chaudhary V, Umar A, Ibrahim AA, Akbar S, Baskoutas S. Paper-based sensors: affordable, versatile, and emerging analyte detection platforms. Anal Methods 2024;16:2777–809. https://doi.org/10.1039/D3AY02258G.
[8] Umapathi R, Park B, Sonwal S, Rani GM, Cho Y, Huh YS. Advances in optical-sensing strategies for the on-site detection of pesticides in agricultural foods, Trends Food. Sci Technol 2022;119:69–89. https://doi.org/10.1016/j.tifs.2021.11.018.
[9] Tai H, Duan Z, Wang Y, Wang S, Jiang Y. Paper-based sensors for gas, humidity, and strain detections: a review. ACS Appl Mater Interfaces 2020;12:31037–53. https://doi.org/10.1021/acsami.0c06435.
[10] Mangotra A, Singh SK. Volatile organic compounds: a threat to the environment and health hazards to living organisms – a review. J Biotechnol 2024;382:51–69. https://doi.org/10.1016/j.jbiotec.2023.12.013.
[11] Shimizu S, Watanabe N, Kataoka T, Shoji T, Abe N, Morishita S, Ichimura H. Pyridine and pyridine derivatives. In: Ullmann's Encyclopedia of Industrial Chemistry; 2000. https://doi.org/10.1002/14356007.a22_399.
[12] Higasio YS, Shoji T. Heterocyclic compounds such as pyrroles, pyridines, pyrollidins, piperdines, indoles, imidazole and pyrazins. Appl Catal A Gen 2001;221:197–207. https://doi.org/10.1016/S0926-860X(01)00815-8.
[13] Allaka TR, Katari NK. Recent Developments in the Synthesis and Applications of Pyridines, Synthesis of pyridine derivatives for diverse biological activity profiles: a review. In: Recent developments in the synthesis and applications of pyridines; 2023. p. 605–25. https://doi.org/10.1016/B978-0-323-91221-1.00005-1.
[14] Pandey RA, Padoley KV, Mukherji SS, Mudliar SN, Vaidya AN, Rajvaidya AS, Subbarao TV. Biotreatment of waste gas containing pyridine in a biofilter. Bioresour Technol 2007;98:2258–67. https://doi.org/10.1016/j.biortech.2006.05.015.
[15] Zalat OA, Elsayed MA. A study on microwave removal of pyridine from wastewater. J Environ Chem Eng 2013;1:137–43. https://doi.org/10.1016/j.jece.2013.04.010.
[16] Liu S-M, Wu C-H, Huang H-J. Toxicity and anaerobic biodegradability of pyridine and its derivatives under sulfidogenic conditions. Chemosphere 1998;36:2345–57. https://doi.org/10.1016/S0045-6535(97)10203-X.
[17] IARC Working Group on the Evaluation of Carcinogenic Risks to Humans. In: Some Industrial Chemicals, vol. 77. Lyon, France: Publisher: International Agency for Research on Cancer; 2000. https://www.ncbi.nlm.nih.gov/books/NBK390856/.
[18] Buron G, Hacquemand R, Pourié G, Jacquot L, Brand G. Effects of pyridine inhalation exposure on olfactory epithelium in mice. Exp Toxicol Pathol 2013;65:159–64. https://doi.org/10.1016/j.etp.2011.08.001.
[19] He F, Qi T, Guo S, Wang H, Zhang Z, Liu R, Zong W. Mechanistic insights into pyridine exposure induced toxicity in model Eisenia fetida species: evidence from whole-animal, cellular, and molecular-based perspectives. Chemosphere 2023;335:139139. https://doi.org/10.1016/j.chemosphere.2023.139139.
[20] Manabu CD, Kishida TM, Watanabe T. Treatment of pyridine in industrial liquid waste by atmospheric DC water plasma. J Hazard Mater 2022;430:128381. https://doi.org/10.1016/j.jhazmat.2022.128381.
[21] Tarannum N, Kumar D. Pyridine: exposure, risk management, and impact on life and environment. In: Chawla M, Singh J, Kaushik RD, editors. Hazardous chemicals. Academic Press; 2025. p. 363–74. https://doi.org/10.1016/B978-0-323-95235-4.00036-0.
[22] Ajslev JZN, Møller JL, Andersen MF, Pirzadeh P, Lingard H. The hierarchy of controls as an approach to visualize the impact of occupational safety and health coordination. Int J Environ Res Publ Health 2022;19:2731. https://doi.org/10.3390/ijerph19052731.
[23] Ridhi R, Saini GSS, Tripathi SK. Study of sensing mechanism of heterocyclic hazardous vapors with Metal Phthalocyanines. Dyes Pigments 2023;116:111328. https://doi.org/10.1016/j.dyepig.2023.111328.
[24] Liu Q, Zhao C, Shao X, Wang W, Ji X. High sensitive pyridine chemiresistive sensors based on azacyclobutane modified perylene bisimide derivatives. Dyes Pigments 2021;185:108902. https://doi.org/10.1016/j.dyepig.2020.108902.
[25] Qin W, Parzuchowski P, Zhang W, Meyerhoff ME. Optical sensor for amine vapors based on Dimer−Monomer equilibrium of indium(III) octaethylporphyrin in a polymeric film. Anal Chem 2003;75:332–40. https://doi.org/10.1021/ac0205356.
[26] Kim JH, Kim S-H. Sub-second pyridine gas detection using a organometal halide perovskite functional dye. Dyes Pigments 2016;134:198–202. https://doi.org/10.1016/j.dyepig.2016.07.015.
[27] Haghighi E, Zeinali S. Nanoporous MIL-101(Cr) as a sensing layer coated on a quartz crystal microbalance (QCM) nanosensor to detect volatile organic compounds (VOCs). RSC Adv 2019;9:24460–70. https://doi.org/10.1039/C9RA04152D.
[28] Xu F, Sun L, Huang P, Sun Y, Zheng Q, Zou Y, Chu H, Yan E, Zhang H, Wang J, Du Y. A pyridine vapor sensor based on metal-organic framework-modified quartz crystal microbalance. Sensor Actuator B Chem 2018;254:872–7. https://doi.org/10.1016/j.snb.2017.07.026.
[29] Liu M, Chen L, Shan P, lian C, Zhang Z, Zhang Y, Tao Z, Xiao X. Pyridine detection using supramolecular organic frameworks incorporating cucurbit[10]uril. ACS Appl Mater Interfaces 2021;13:7434–42. https://doi.org/10.1021/acsami.0c20292.
[30] Bairi P, Minami K, Nakanishi W, Hill JP, Ariga K, Shrestha LK. Hierarchically structured fullerene C_{70} cube for sensing volatile aromatic solvent vapors. ACS Nano 2016;10:6631–7. https://doi.org/10.1021/acsnano.6b01544.
[31] Khaing Oo MK, Guo Y, Reddy K, Liu J, Fan X. Ultrasensitive vapor detection with surface-enhanced Raman scattering-active gold nanoparticle immobilized flow-through multihole capillaries. Anal Chem 2012;84:3376–81. https://doi.org/10.1021/ac300175v.
[32] Zhao K, Dong L, Zheng Y, Deng G, Li Z, Qu S, Chen K, Wu J. Optimization of light-analyte interaction in Si_3N_4/polymer hybrid waveguide for sensitive sensing of pyridine vapor with ppb-level detection limit. Sensor Actuator B Chem 2023;377:133104. https://doi.org/10.1016/j.snb.2022.133104.
[33] Thompson AC, Lee KS, Lewis NS. Strain-based chemiresistive polymer-coated graphene vapor sensors. ACS Omega 2022;7:10765–74. https://doi.org/10.1021/acsomega.2c00543.
[34] Younis M, Long J, Peng SQ, Wang XS, Chai C, Bogliotti N, Huang MH. Reversible transformation between azo and azonium bond other than photoisomerization of azo bond in main-chain polyazobenzenes. J Phys Chem Lett 2021;12:3655–61. https://doi.org/10.1021/acs.jpclett.1c00750.
[35] Rochat S, Swager TM. Fluorescence sensing of amine vapors using a cationic conjugated polymer combined with various anions. Angew Chem Int Ed 2014;53:9792–6. https://doi.org/10.1002/anie.201404439.
[36] Dai Z-Y, Song L, Chen J-E, Jin D-F, Jin H-X, Lin Guo X, Shena H-Y, Chai W-X. Smart-responsive luminescence and VOC sensing application of a copper(I) cluster with a novel $P_2CuI_2CuN_2$ core. J Mater Chem C 2025;12:7234–44. https://doi.org/10.1039/D4TC05038J.
[37] Ermakova EV, Arslanov VV, Bretonnière Y, Michel C, Bessmertnykh-Lemeune A. Supramolecular assembly of phosphonatesubstituted porphyrins in Langmuir layers and Langmuir–Schäfer films: structural studies and selective sensing of pyridine vapors. J Mater Chem C 2025;12:4791–806. https://doi.org/10.1039/D4TC04449E.
[38] Kondo S, Yoshimura N, Kobayashi A, Charith Kuruppu KD, Sameera WMC, Fujii S, Yoshida M, Kato M. Vapoluminescent thin-film with unsaturated copper(I) complex for rapid light-on sensing of N-heteroaromatic vapour. J Mater Chem C 2024;12:1799–808. https://doi.org/10.1039/D3TC03571A.
[39] Kusumoto S, Inaba K, Suda H, Nakaya M, Tokunaga R, Thuéry P, Haruki R, Kanazawa T, Nozawa S, Kim Y, Hayami S, Koide Y. Cooperative spin-state switching and vapochromism of mononuclear Ni(II) complexes by pyridine

coordination/decoordination. Inorg Chem 2023;62:16222–7. https://doi.org/10.1021/acs.inorgchem.3c02776.
[40] Murakami T, Homma T, Masuno A, Okazaki M, Ohta S. Color-change behavior of a bis(benzimidazole)-coordinated nickel-dichlorido complex induced by the adsorption of pyridine or ammonia vapor, Transit. Met Chem 2024;49:229–35. https://doi.org/10.1007/s11243-024-00576-9.
[41] Lv Y, Zhang Y, Du Y, Xu J, Wang J. A novel porphyrin-containing polyimide nanofibrous membrane for colorimetric and fluorometric detection of pyridine vapor. Sensors 2013;13:15758–69. https://doi.org/10.3390/s131115758.
[42] Tang S-Y, Song L, Jia Y-F, Xu W-Z, Yang Y-X, Sun L-J, Shen H-Y, Chai W-X. Three heteroleptic copper(I) complexes with $[Cu(P\ P)N_2]^+$ structure and their fluorescence sensing for VOCs. Appl Organomet Chem 2023;37:e7242. https://doi.org/10.1002/aoc.7242.
[43] Elosua C, Bariain C, Matias IR, Rodriguez A, Colacio E, Salinas-Castillo A, Segura-Carretero A, Fernandez-Gutiérrez A. Pyridine vapors detection by an optical fibre sensor. Sensors 2008;8:847–59. https://doi.org/10.3390/s8020847.
[44] Oliveri IP, Di Bella S. Lewis Acidic Zinc(II) complexes of tetradentate ligands as building blocks for responsive assembled supramolecular structures. Chemistry 2023;5:119–37. https://doi.org/10.3390/chemistry5010010.
[45] Di Bella S. Lewis acidic zinc(II) salen-type Schiff-base complexes: sensing properties and responsive nanostructures. Dalton Trans 2021;50:6050–63. https://doi.org/10.1039/D1DT00949D.
[46] Consiglio G, Oliveri IP, Failla S, Di Bella S. On the aggregation and sensing properties of zinc(II) schiff-base complexes of salen-type ligands. Molecules 2019;24:2514. https://doi.org/10.3390/molecules24132514.
[47] Forte G, Oliveri IP, Consiglio G, Failla S, Di Bella S. On the Lewis acidic character of bis(salicylaldiminato)zinc(II) Schiff-base complexes: a computational and experimental investigation on a series of compounds varying the bridging diamine. Dalton Trans 2017;46:4571–81. https://doi.org/10.1039/C7DT00574A.
[48] Gaeta M, Oliveri IP, Munzi G, Lo Presti F, Di Bella S. Stimuli-responsive properties of a Zinc (II) salen-type Schiff-base complex and vapochromic detection of volatile organic compounds. Inorg Chem 2024;63:3850–8. https://doi.org/10.1021/acs.inorgchem.3c04165.
[49] Attinà A, Oliveri IP, Di Bella S. Detection of volatile primary aliphatic amines: highly selective and sensitive vapoluminescent sensing of *n*-butylamine. Sensor Actuator B Chem 2024;119:136414. https://doi.org/10.1016/j.snb.2024.136414.
[50] Attinà A, Oliveri IP, Gaeta M, Di Bella S. Sensitive and discriminative fluorescent detection of volatile primary aliphatic diamine vapors from monoamines. Molecules 2024;29:5947. https://doi.org/10.3390/molecules29245947.
[51] Oliveri IP, Malandrino G, Di Bella S. Phase transition and vapochromism in molecular assemblies of a polymorphic zinc(II) Schiff-base complex. Inorg Chem 2014;53:9771–7. https://doi.org/10.1021/ic5013632.
[52] Kurz H, Hils C, Timm J, Hörner G, Greiner A, Marschall R, Schmalz H, Weber B. Self-Assembled fluorescent block copolymer micelles with responsive emission. Angew Chem Int Ed 2022;61:e202117570. https://doi.org/10.1002/anie.202117570.
[53] Strianese M, Guarnieri D, Lamberti M, Landi A, Peluso A, Pellecchia C. Fluorescent *salen*-type Zn(II) complexes as probes for detecting hydrogen sulfide and its anion: bioimaging applications. Inorg Chem 2020;59:15977–86. https://doi.org/10.1021/acs.inorgchem.0c02499.
[54] Yan X, Song X, Mu X, Wang Y. Mechanochromic luminescence based on a phthalonitrile-bridging salophen zinc(II) complex. New J Chem 2019;43:15886–91. https://doi.org/10.1039/C9NJ03704G.
[55] Song X, Yu H, Yan X, Zhang Y, Miao Y, Ye K, Wang Y. A luminescent benzothiadiazole-bridging bis(salicylaldiminato)zinc(II) complex with mechanochromic and organogelation properties. Dalton Trans 2018;47:6146–55. https://doi.org/10.1039/C8DT00665B.
[56] Piccinno M, Angulo-Pachón CA, Ballester P, Escuder B, Dalla Cort A. Rational design of a supramolecular gel based on a Zn(II)–salophen bis-dipeptide derivative. RSC Adv 2016;6:57306–9. https://doi.org/10.1039/C6RA12731B.
[57] Hui JK-H, Yu Z, MacLachlan MJ. Supramolecular assembly of Zinc salphen complexes: access to metal-containing gels and nanofibers. Angew Chem, Int Ed 2007;46:7980–3. https://doi.org/10.1002/anie.200702680.
[58] Oliveri IP, Consiglio G, Munzi G, Failla S, Di Bella S. Deaggregation properties and transmetalation studies of a zinc(ii) salen-type Schiff-base complex. Dalton Trans 2022;51:11859–67. https://doi.org/10.1039/D2DT01448C.
[59] National Institute for occupational safety and health, pyridine. https://www.cdc.gov/niosh/idlh/110861.html. [Accessed 22 April 2025].
[60] Mazur F, Han Z, Tjandra AD, Chandrawati R. Digitalization of colorimetric sensor technologies for food safety. Adv Mater 2024;36:2404274. https://doi.org/10.1002/adma.202404274.
[61] Koschan A, Abidi MA. Digital color image processing. John Wiley & Sons.; 2008. p. 37–70. https://doi.org/10.1002/9780470230367.ch3 [Chapter 3], Color Spaces and Color Distances.
[62] Gao Y, Liang J, Yang J. Color palette generation from digital images: a review. Color Res Appl 2024:1–16. https://doi.org/10.1002/col.22975.
[63] Chavolla E, Zaldivar D, Cuevas E, Perez MA. Color spaces advantages and disadvantages in image color clustering segmentation. In: Hassanien A, Oliva D, editors. Advances in Soft Computing and Machine Learning in Image Processing. Studies in Computational Intelligence, vol. 730. Springer International Publishing; 2018. p. 3–22. https://doi.org/10.1007/978-3-319-63754-9_1.
[64] Mokrzycki W, Tatol M. M. Colour difference ΔE-A survey, Mach. Graph Vis 2011;20:383–411. https://dl.acm.org/toc/mgvij/2011/20/4.
[65] Rao Padma, Ankam S, Ansari M, Gavane AG, Kumar A, Pandit VI, Nema P. Monitoring of hydrocarbon emissions in a petroleum refinery. Environ Monit Assess 2005;108:123–32. https://doi.org/10.1007/s10661-005-3961-x.
[66] Oliveri IP, Maccarrone G, Di Bella S. A Lewis basicity scale in dichloromethane for amines and common nonprotogenic solvents using a Zinc(II) schiff-base complex as reference Lewis acid. J Org Chem 2011;76:8879–84. https://doi.org/10.1021/jo2016218.